2882 J. Med. Chem. 2010, 53, 2882–2891
DOI: 10.1021/jm901858n

Journal of Medicinal Chemistry Article

Radiosynthesis and Bioimaging of the Tuberculosis Chemotherapeutics Isoniazid, Rifampicin and Pyrazinamide in Baboons

Li Liu,[†] Youwen Xu,[‡] Colleen Shea,[‡] Joanna S. Fowler,[‡] Jacob M. Hooker,*[,‡,∥] and Peter J. Tonge*[,†]

[†]*Institute for Chemical Biology & Drug Discovery, Department of Chemistry, Stony Brook University, Stony Brook, New York 11794-3400, and* [‡]*Medical Department, Brookhaven National Laboratory, Upton, New York 11973-5000.* [∥]*Present address: Athinoula A. Martinos Center for Biomedical Imaging, Charlestown, Massachusetts 02129.*

Received December 17, 2009

The front-line tuberculosis (TB) chemotherapeutics isoniazid (INH), rifampicin (RIF), and pyrazinamide (PZA) have been labeled with carbon-11 and the biodistribution of each labeled drug has been determined in baboons using positron emission tomography (PET). Each radiosynthesis and formulation has been accomplished in 1 h, using [^{11}C]CH_3I to label RIF and [^{11}C]HCN to label INH and PZA. Following iv administration, INH, PZA, RIF, and/or their radiolabeled metabolites clear rapidly from many tissues; however, INH, PZA, and/or their radiolabeled metabolites accumulate in the bladder while RIF and/or its radiolabeled metabolites accumulates in the liver and gall bladder, consistent with the known routes of excretion of the drugs. In addition, the biodistribution data demonstrate that the ability of the three drugs and their radiolabeled metabolites to cross the blood−brain barrier decreases in the order PZA > INH > RIF, although in all cases the estimated drug concentrations are greater than the minimum inhibitory concentration (MIC) values for inhibiting bacterial growth of *Mycobacterium tuberculosis* (MTB). The pharmacokinetic (PK) and drug distribution data have important implications for treatment of disseminated TB in the brain and pave the way for imaging the distribution of the pathogen in vivo.

Introduction

The dose and duration of treatment of antibiotics is normally established using plasma pharmacokinetic (PK[a]) data together with information on drug efficacy once treatment has been initiated. Although plasma drug concentration is an important guide for establishing treatment protocols, recent studies indicate that the distribution of antibiotics in tissues is a more critical determinant and predictive factor for their activity.[1,2] This is because most drugs exert their bactericidal effects at the site of infection rather than in the plasma and because drug equilibration between plasma and infection site cannot always be achieved.[1,2] Failure to reach optimal drug concentration at the site of infection may result in therapeutic failure and trigger bacterial resistance.[1] Therefore, the Food and Drug Administration (FDA) now requires clinical studies of tissue drug distribution at uninfected and infected sites.[1] Positron emission tomography (PET), which images drugs and other molecules labeled with positron-emitting isotopes, provides a method of acquiring quantitative information on the dynamics of drug absorption, distribution, and elimination in a living animal or human. Together with advances in the development of methods for labeling drug molecules and other organic compounds with carbon-11 (half-life: 20.4 min), PET is emerging as a powerful alternative to ex vivo distribution studies using laboratory animals which sample a single time point per animal. Indeed, PET can map three-dimensional tissue distribution over time noninvasively.[3] It is also complementary to clinical microdialysis (MD) and magnetic resonance spectroscopy (MRS) in terms of acquiring information on the tissue distribution of different chemical species.[2] In addition, the methodology developed for imaging drug distribution in laboratory animals using PET can be readily translated to humans.[3]

More than two million deaths every year are attributed to infection with *Mycobacterium tuberculosis* (MTB) and the World Health Organization (WHO) has estimated that one-third of the world's population is infected with this pathogen.[4−6] While many bacterial infections are treated using a 1−2 week course of monotherapy, the treatment of tuberculosis (TB) requires the use of multiple antibiotics over a 6−9 month period, dramatically increasing the risk of noncompliance and enhancing the emergence of resistance.[7] The current treatment regime for drug-sensitive TB involves the use of isoniazid (INH), rifampicin (RIF), pyrazinamide (PZA), and ethambutol (EMB) or streptomycin for two months, followed by four months of continued dosing with INH and RIF. This regime has been used for decades and is primarily based on PK studies in serum combined with historical data on the efficacy

*To whom correspondence should be addressed. For P.J.T.: phone, (631) 632 7907; fax, (631) 632 7960; E-mail, peter.tonge@sunysb.edu. For J.M.H.: phone, (617) 726 6596; fax, (617) 726 7422; E-mail, hooker@nmr.mgh.harvard.edu.

[a]Abbreviations: TB, tuberculosis; INH, isoniazid; RIF, rifampicin; PZA, pyrazinamide; MIC, minimum inhibitory concentration; PK, pharmacokinetic; FDA, Food and Drug Administration; PET, positron emission tomography; MD, microdialysis; MRS, magnetic resonance spectroscopy; MTB, *Mycobacterium tuberculosis*; WHO, World Health Organization; EMB, ethambutol; CNS, central nervous system; CSF, cerebrospinal fluid; PPB, plasma protein binding; TAC, time−activity curve; AUC, area under the curve; ROI, region-of-interest; FBP, filtered back projection; %ID/cc, % of injected dose per cubic centimeter; HPLC, high performance liquid chromatography; RCY, radiochemical yield; DCY, decay-corrected yield.

 Published on Web 03/08/2010

Scheme 1. Radiosynthesis of [^{11}C]RIF

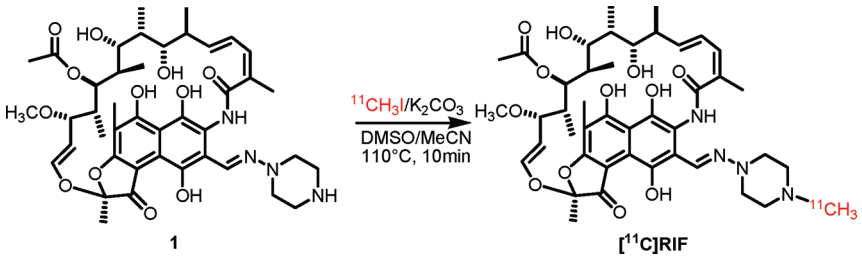

of treatment.[8] TB infection most commonly occurs through inhalation of live bacteria, and thus the primary site of infection in humans are the lungs. However, MTB can also disseminate via the bloodstream and infect other organs in the body. In particular, MTB infection of the brain (central nervous system TB, CNS TB) can occur. CNS TB is presented in many forms including tuberculous meningitis, cerebral tuberculomas without meningitis, and spinal TB.[9] CNS TB is particularly difficult to manage because the pathogenesis, diagnosis, and treatment of this form of TB infection has not been as intensively studied as pulmonary TB, and there is little data to guide treatment options.[9,10] Current treatment for CNS TB normally follows the same format as that used for treating pulmonary TB and involves an intensive phase of treatment followed by a continuation phase.[9,10] Thus, both INH and RIF are included in the treatment based on their potent activity against pulmonary TB infection and, in the case of INH, the significant levels of this drug that can be detected in the cerebrospinal fluid (CSF). In addition, although high concentrations of PZA can be detected in the CSF, the importance of this drug for treating CNS TB is largely unknown.[9,10] Although measurement of CSF drug concentration through lumbar puncture is a good indication of drug availability in brain, it would be advantageous to be able to measure brain drug distribution noninvasively and more accurately because a ventriculo-lumbar concentration gradient is often observed and the distribution of drugs in each compartment of the CNS is not homogeneous.[11]

Here we present a PET imaging study of carbon-11 labeled RIF, INH, and PZA in baboons in order to provide more direct insight into the PK and biodistribution of drugs commonly used to treat TB. These studies in healthy baboons are a prelude to imaging experiments in infected animals and humans and should ultimately be useful in evaluating new TB treatment regimes, especially for disseminated forms of the disease such as CNS TB where the ability to evaluate drug availability at the site of infection may be limited.

Using PET, we find that all three drugs and/or their radiolabeled metabolites are cleared rapidly from the lungs. In addition, their accumulations are consistent with the mechanism of excretion of each drug. We also find that the organ distribution of each drug differs by 1−1000 fold from the plasma drug distribution. All of the three injected drugs reached higher concentrations in the lung than the plasma over the time course of the experiment. In addition, we find that the ability of the drugs to penetrate the blood−brain barrier decreases in the order PZA > INH > RIF. Estimates based on the weight of the baboon, a standard drug dose and the assumption that the positron signal derives primarily from the intact drug indicates that the concentrations of RIF, INH, and PZA in the lungs are at least 10, 10, and 1−3 times higher, respectively, than the minimum inhibitory concentration (MIC) values for these drugs against MTB. Estimates of drug concentrations in the brain using the same assumptions outlined above suggest that the concentrations of RIF and INH are 3−4 and >10 times higher than their MIC values, while the concentration of PZA is similar to or slightly higher than its MIC. These data have important implications for the treatment of TB and set the scene for additional studies in humans.

Results and Discussion

Radiosynthesis of [^{11}C]RIF. The radiolabeling of the RIF piperazine moiety with [^{11}C]CH_3I was accomplished by using potassium carbonate and a combination of DMSO and MeCN (Scheme 1). Although the conditions for labeling a piperazine with [^{11}C]CH_3I have been published before,[12] we were concerned that other nucleophilic sites could also be alkylated (e.g., *O*-methylation of the phenolic oxygens). Consequently, we explored a range of non-nucleophilic organic and inorganic bases in combination with polar aprotic solvents in order to identify conditions that would give the required rate, radiochemical yield, and regioselectivity (i.e., *N*-methylation). These studies resulted in the use of potassium carbonate as the base and a combination of DMSO and MeCN as the solvent (Scheme 1). The [^{11}C]RIF was subsequently purified by high performance liquid chromatography (HPLC) using a semipreparative Phenomenex Luna C-18 column (250 × 10, 5 μm), and 100 mg of ascorbic acid was added to the product solution prior to concentration in vacuo in order to prevent oxidation. In the optimized reaction scheme, the average decay-corrected yield (DCY), calculated from [^{11}C]CH_3I, was 15−25% in a total synthesis time of 50 min. Analytical HPLC and TLC demonstrated that the radiolabeled product was over 99% radiochemically pure, with a specific activity of 580 mCi/μmol at the time of delivery to the animal.

Radiosynthesis of [^{11}C]INH. The synthesis of [^{11}C]INH was accomplished in three steps beginning from [^{11}C]HCN. The first step involved treating iodopyridine (**2**) with [^{11}C]HCN in a DMSO reaction mixture catalyzed by tetrakis(triphenylphosphine)palladium(0) (Scheme 2) for 5 min to form [^{11}C]cyanopyridine (**3**). This method was adapted from previously reported radiolabeling of an aromatic ring with [^{11}C]HCN,[13] and gave 90% radiochemical yield (RCY) as determined by HPLC. The subsequent hydrazine hydrolysis of the cyanide was accomplished in two steps, which involved a nucleophilic attack by hydrazine and subsequent hydrolysis of the imine by water. This procedure was a modification of a published method,[14] which used NaY zeolite as the catalyst to hydrolyze the aromatic cyano group without adding acetic acid to drive the reaction. Initial studies indicated that the hydrolysis step was too slow to be useful with carbon-11 (approximately 60 min

Scheme 2. Radiosynthesis of [^{11}C]INH

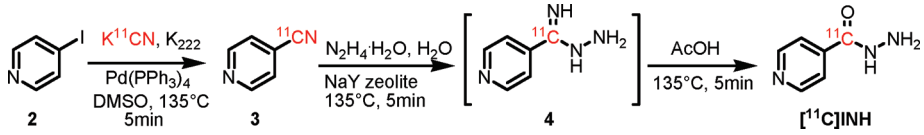

Scheme 3. Radiosynthesis of [^{11}C]PZA

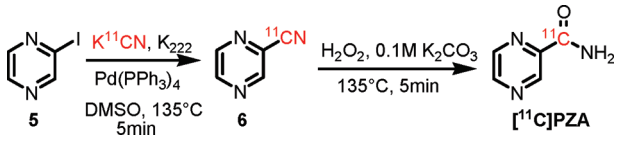

at 180 °C). However, because mass spectrometry revealed the formation of intermediate (**4**) together with the complete consumption of **3** within the first 5 min of the reaction, acetic acid was added to promote hydrolysis of the intermediate. Using this two-step procedure, the combined hydrazine addition and hydrolysis time of **3** was reduced to 10 min. The final product was formed with an average 45−50% DCY (calculated from [^{11}C]HCN) in a total synthesis time of 50 min. Isonicotinamide was the only major byproduct, but with optimization of the ratio between hydrazine, water, and acetic acid (3:3:1), formation of this adduct could be reduced to less than 15% of the desired product. [^{11}C]INH was purified by semipreparative HPLC, and the amount of hydrazine in the sample, that initially coeluted with [^{11}C]INH, was reduced by evacuation of the sample on the rotary evaporator for 10 min. The average amount of hydrazine present in the injected solution was 8.2 μg/mL (~10.0 μg/injection) as determined by an analytical assay, which was adapted from a previous report.[15] Analytical HPLC and TLC were used to demonstrate that the radiolabeled product was over 99% radiochemically pure, with a specific activity of 140−165 mCi/μmol at the time of delivery.

Radiosynthesis of [^{11}C]PZA. The radiosynthesis of [^{11}C]PZA is shown in Scheme 3. Initially, [^{11}C]cyanopyrazine (**6**) was generated with a 90% RCY in 5 min from 2-iodopyrazine (**5**) and [^{11}C]HCN using tetrakis(triphenylphosphine)palladium-(0) as the catalyst under the same reaction conditions as those used for [^{11}C]INH.[13] Subsequent hydrolysis of the cyano group was accomplished in an additional 5 min by treating **6** with hydrogen peroxide under basic conditions. The overall DCY was 50−55% (calculated from [^{11}C]HCN) in a total synthesis time of 45 min. An unidentified volatile compound coeluted with the [^{11}C]PZA product during HPLC purification, however, this was removed during concentration of the product in vacuo. Analytical HPLC and TLC demonstrated that the radiolabeled product was over 99% radiochemically pure, with a specific activity of 120−150 mCi/μmol at the time of delivery.

LogD and Plasma Protein Binding (PPB). The lipophilicity (logD) and PPB of each drug was determined using the radiolabel to report on drug concentration. The results are presented in Table 1 and are similar to literature values reported elsewhere.[16,17]

Brain PET Imaging in Anesthetized Baboons. PET imaging studies were performed with [^{11}C]RIF, [^{11}C]INH, and [^{11}C]PZA to determine brain penetration and distribution. Time−activity curves (TACs) (Figure 1a) were generated from the image data, which was acquired for 90 min following iv administration of each radiolabeled drug. Area under the curves (AUCs)

Table 1. LogD and PPB Determination

	LogD	PPB,[a] %
RIF	1.67	27.32
INH	nd[b]	94.63
PZA	−0.41	91.32

[a] Value expressed as % of free fraction in plasma. [b] Octanol−water partitioning was highly variable.

(Figure 1b) were produced by integrating TACs as a function of time and dose corrected coronal images (Figure 1c) were generated by sum from 15 to 90 min. Regions-of-interest (ROIs) were drawn manually.

These PET studies are the first in which dynamic TB drug concentrations have been measured in whole brain tissue in a living animal. Figure 1 clearly demonstrates that the ability of the drugs and their radiolabeled metabolites to penetrate the blood−brain barrier decreases in the order PZA > INH > RIF. The [^{11}C]RIF TAC, AUC, and image (Figure 1) showed that RIF and/or its radiolabeled metabolites poorly penetrate the blood−brain barrier in healthy baboons, consistent with previous studies in which the concentration of iv delivered RIF in human CSF was measured. Our studies demonstrate a higher RIF concentration in brain tissue than that observed in the CSF.[18] The concentration of injected [^{11}C]RIF in the whole brain area was monitored over the 90 min scanning period with a $C_{30\ min}$ = 0.000642%-ID/cc (1.09 μg/mL), $C_{60\ min}$ = 0.000536%ID/cc (0.912 μg/mL), and $C_{90\ min}$ = 0.000710%ID/cc (1.21 μg/mL). In parentheses we have estimated the expected concentration of RIF in the baboon brain based on the weight of the baboon (17 kg), the recommended daily dose for a human adult (10 mg/kg) and the assumption that the positron signal derives primarily from the intact drug. Thus, for a 17 kg baboon the injected dose is 170 mg and, for example, at 30 min the concentration in the brain is estimated to be 0.000642% of 170 mg in each cubic centimeter which is 1.09 μg/mL. The anticipated concentration of RIF in the baboon brain is therefore 3−4 times above the MTB MIC for this compound, supporting the use of RIF for treating CNS TB infections.[9,18] The concentrations of RIF observed in our study are similar to the value of 0.87 μg/g determined in monkeys 6 h after iv administration of [^{14}C]RIF,[19] which suggests that the observed level of RIF could persist for several hours in brain tissue. In addition, although studies in mice revealed a much higher RIF brain tissue concentration of 10.25 μg/mL 3−7 h after ip administration,[20] the latter measurements were made with a 100 mg/kg dose of RIF and thus are likely similar to the concentrations reported from our PET study if our estimates were based on a 100 mg/kg dose. Finally, Thomas and co-workers resected human brain tissue around tumors and determined a RIF concentration of 0.29 μg/mL following iv infusion of 600 mg of RIF in 500 mL saline over 3 h.[21] Thus, the concentrations of RIF determined by PET imaging the distribution of [^{11}C]RIF in healthy baboons are similar to those observed in mice and monkeys, while the ~3.5-fold difference between our values

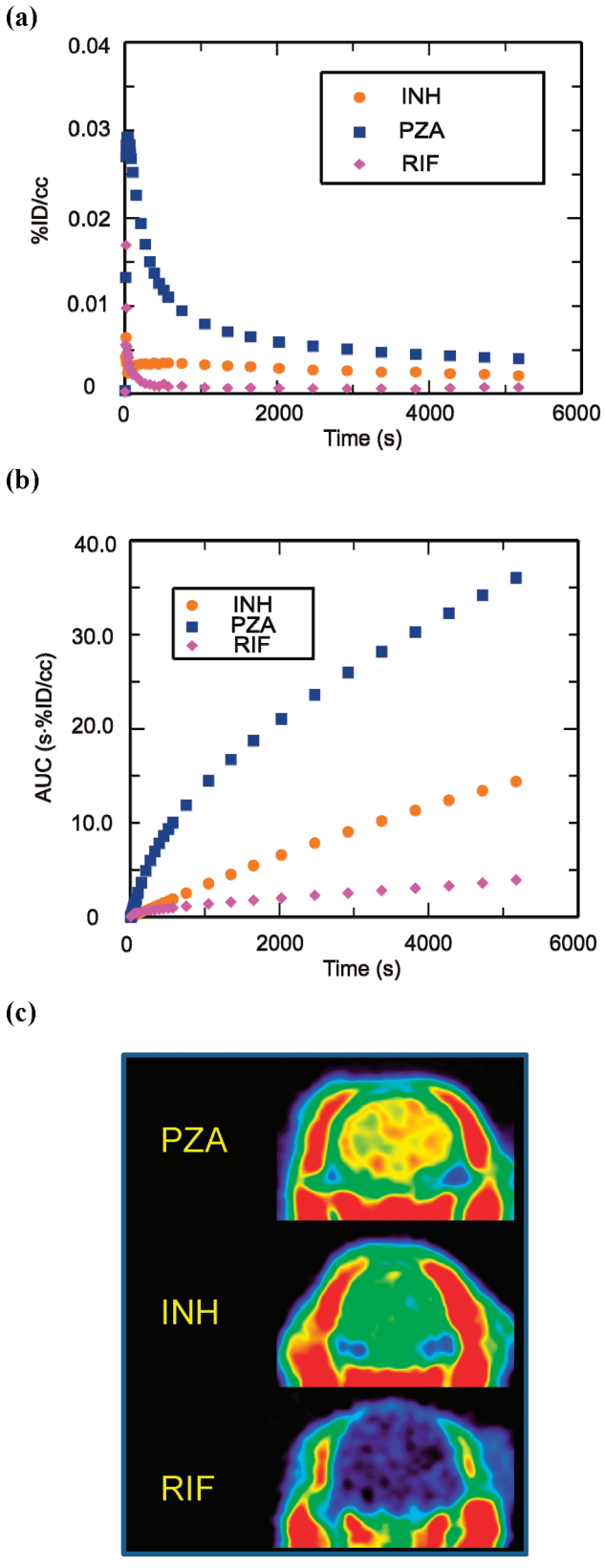

Figure 1. Blood−brain barrier penetration, brain tissue bioavailability, and TACs for [^{11}C]PZA, [^{11}C]INH, and [^{11}C]RIF. (a) TACs generated from the image acquired after iv administration of each drug in baboons by manually drawing the ROIs. (b) Whole-brain regions of interest were used to generate TACs for each labeled drug. The resulting curves were integrated as a function of time to produce AUC plots. (c) Dose corrected coronal images summed over frames 24−35 (15−90 min). The NIH color scale was used to represent relative radioactivity concentration.

and that determined by resecting brain tissue could be due to the limited sampling region in the latter experiments. Although the studies with [^{14}C]RIF do provide information on drug distribution, this is only at a single time point, whereas the PET imaging experiments provide dynamic data from 0 to 90 min. Importantly, the PET studies are noninvasive and thus can be readily applied to determining RIF concentration and distribution in humans.

The [^{11}C]INH TAC, AUC, and image (Figure 1) showed a higher initial brain penetration and tissue accumulation when compared to RIF, consistent with CSF analysis in humans.[22,23] The concentration of injected [^{11}C]INH in the whole brain area was monitored after iv administration (Figure 1a) and gave $C_{30\ min}$ = 0.00299%ID/cc (2.54 μg/mL), $C_{60\ min}$ = 0.00248%ID/cc (2.11 μg/mL), and $C_{90\ min}$ = 0.00206%ID/cc (1.75 μg/mL). Again, concentrations in μg/mL are estimated based on the weight of the baboon, the recommended daily dose for a human adult which is 5 mg/kg, and the assumption that the positron signal derives primarily from the intact drug. Thus, the calculated INH concentration is more than 10 times above the MIC of this compound against MTB and hence INH should be a suitable therapy for CNS TB infection as recommended,[9] with the caveat that INH must be used with another drug because INH-resistant mutants emerge quickly during monotherapy.[24] Concentrations estimated from our [^{11}C]INH study are similar to those determined in mice using [^{14}C]INH in which a 10 mg/kg sc dose gave concentrations of 4.4 and 3.2 μg/g at 30 and 60 min, respectively.[25] However, studies in cats in which [^{14}C]INH was administered ip revealed much lower penetration of INH into the brain, with a calculated INH concentration of only 0.02 μg/g.[26,27] The lower brain concentration of INH determined in cats compared to our baboon study could reflect interspecies differences and/or the different routes of administration that were used. Finally, although the observed CSF concentrations in humans from two experiments are contradictory (1.9 μg/mL with 8.5 mg/kg oral dose at 2 h[28] and 0.31 μg/mL with 108.7 mg oral dose at 1 h[22]), it is clear that the INH concentration in brain tissue is equal to, or greater than, the concentration in the CSF.

The [^{11}C]PZA TAC, AUC, and image indicated excellent penetration of PZA into healthy brain tissue in vivo (Figure 1). This result is consistent with CSF analysis in humans in which the PZA concentration in the CSF exceeded that in the serum.[29] For example, in the brain, the $C_{60\ min}$ was 0.00463%ID/cc while in the plasma the $C_{60\ min}$ was 0.00272%ID/cc. The concentration of [^{11}C]PZA in the whole brain area decreased following iv administration, with $C_{30\ min}$ = 0.00619%ID/cc (21.05 μg/mL), $C_{60\ min}$ = 0.00463%ID/cc (15.74 μg/mL), and $C_{90\ min}$ = 0.00403%ID/cc (13.70 μg/mL). As above, concentrations in μg/mL are estimated based on the weight of the baboon, the recommended daily dose for a human adult which is 20 mg/kg and the assumption that the positron signal derives primarily from the intact drug. We believe that this is the first study of PZA distribution in the primate brain. Studies with rats conducted by Wu and co-workers using MD gave similar brain tissue concentrations using a similar dose administered iv,[30] while in patients with inflamed meninges, the CSF concentration of PZA was 50 μg/mL following a single 3 g oral dose.[29] The calculated PZA concentration at different time points from our baboon study is similar to or slightly greater than the MIC value for this drug against MTB.

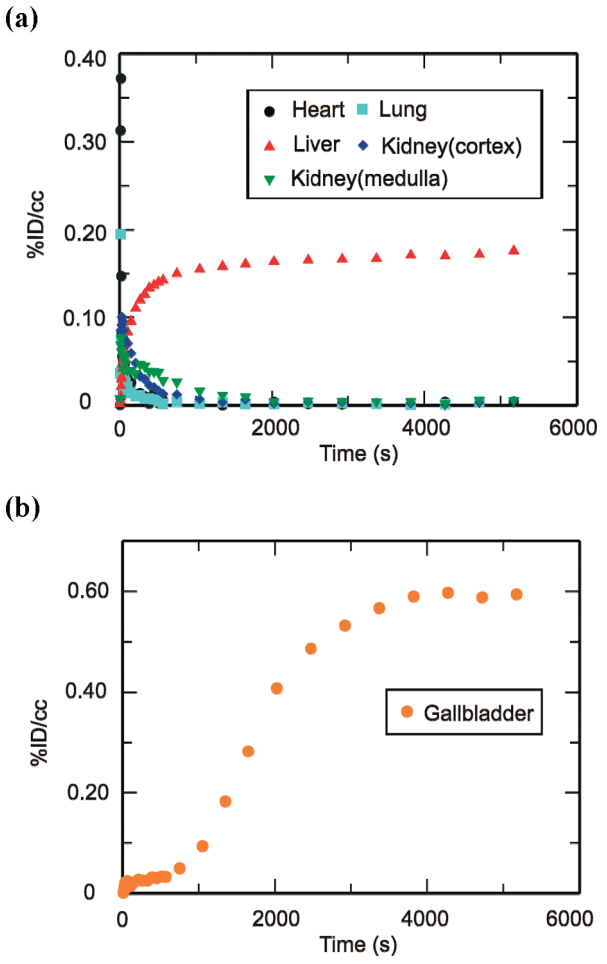

Figure 2. TACs for [^{11}C]RIF in the (a) heart, lungs, liver, kidneys, and (b) gallbladder. Peripheral organ distribution following torso PET imaging of [^{11}C]RIF administered iv to anesthetized baboons. TACs were generated from the image acquired after iv administration of each drug in baboons by manually drawing the ROIs.

Torso PET Imaging in Anesthetized Baboons. PET imaging studies were performed with [^{11}C]RIF, [^{11}C]INH, and [^{11}C]PZA to determine their peripheral organ distribution. The TACs (Figures 2, 3 and 4) were generated from the image acquired after iv administration of each drug to baboons by manually drawing the ROIs.

[^{11}C]RIF administered iv had moderate distribution in the heart, lung, and kidneys and was concentrated in the liver and gallbladder (Figure 2). The concentration of RIF in μg/mL at 15, 30, 60, and 90 min has been estimated based on the weight of the baboon, the recommended dose of RIF, and assumption that the positron signal derives primarily from the intact drug (Table 2). The anticipated concentration of RIF in the lungs is more than 10 times above the MTB MIC for this compound and hence RIF should be a suitable therapy for TB infections as recommended by the American Thoracic Society.[8] In most organs, the concentration of injected RIF exceeds that in plasma over the study period except for the cortex of the kidney at 60 min. Although Nitti et al. have reported a PK study of RIF administered iv from 15 min to 12 h,[31] these results are difficult to compare with our own because in their case the drug was infused over a 3 h period. In addition, Furesz and co-workers used samples obtained by biopsy to determine the concentration of orally administered RIF in the organs and body fluids of patients

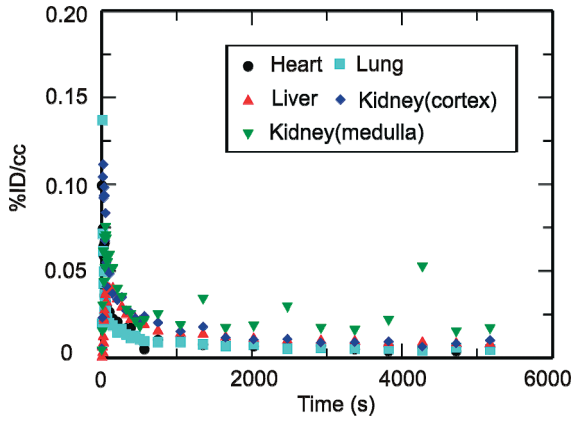

Figure 3. TACs for [^{11}C]INH in the heart, lungs, liver, and kidneys. Peripheral organ distribution following torso PET imaging of [^{11}C]INH administered iv to anesthetized baboons. TACs were generated from the image acquired after iv administration of each drug in baboons by manually drawing the ROIs.

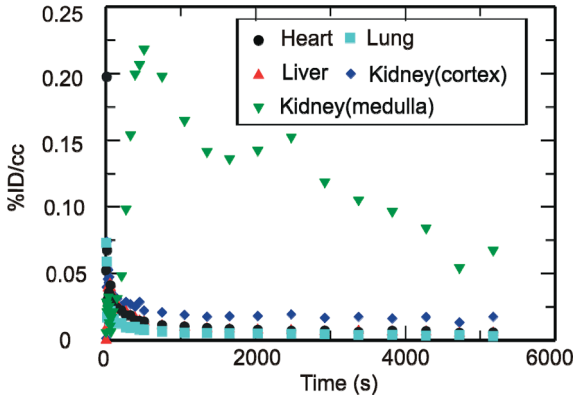

Figure 4. TACs for [^{11}C]PZA in the heart, lungs, liver, and kidneys. Peripheral organ distribution following torso PET imaging of [^{11}C]PZA administered iv to anesthetized baboons. TACs were generated from the image acquired after iv administration of each drug in baboons by manually drawing the ROIs.

with diseases that are presumed not to affect the absorption and elimination of RIF.[32] Although their data do not show concentrations before 90 min, the relative abundance of RIF in each organ and body fluid is quite similar to our own measurements and demonstrates that in most cases the concentration of drug in the organs exceeds that in the serum. In their study, the bile concentration after a 150 mg oral dose is up to 538.5 μg/mL at 3−5 h, while the concentration in the liver is between 22 and 35 μg/mL, which is several fold smaller than our estimated liver concentration. This result may suggest that RIF is cleared quickly from the liver between 1.5 and 3 h post administration. Our data can also be compared with the tissue distribution of RIF in monkeys performed 6 h after iv administration of [^{14}C]RIF. In the latter experiment, the liver still had the highest concentration (60.41 μg/g), while the heart, lung, and kidney retained some drug (10.11, 8.32, and 14.69 μg/g, respectively).[19] Finally, a semiquantitative evaluation of whole body RIF distribution in mice using iv injected [^{14}C]RIF suggested a similar drug distribution compared to our own studies except that the difference between the liver and other organs was not as large.[33]

The tissue distribution of injected [^{11}C]INH is shown in Figure 3 where it is clear that INH and/or its radiolabeled

Table 2. Distribution of [^{11}C]RIF Administered iv to Baboons[a]

min after administration	heart	lung	liver	kidney cortex	kidney medulla	gallbladder	plasma
15	0.0043	0.003	0.1523	0.0093	0.0214	0.0714	0.00165
	(7.28)	(5.03)	(258.98)	(15.79)	(36.39)	(121.40)	(2.81)
30	0.0031	0.0017	0.1624	0.0037	0.0068	0.3449	0.00088
	(5.28)	(2.83)	(276.12)	(6.34)	(11.63)	(586.34)	(1.50)
60	0.0011	0.0015	0.1694	0.0003	0.004	0.5784	0.00067
	(1.93)	(2.53)	(288.05)	(0.43)	(6.73)	(983.24)	(1.14)
90	0.004	0.0040[b]	0.1763	0.0048	0.0056	0.5941	0.00068
	(6.80)	(6.78)	(299.73)	(8.19)	(9.44)	(1009.99)	(1.16)

[a] Values given are [%ID/cc] while the values in parentheses are concentration of drug in μg/mL calculated assuming a 10 mg/kg dose and a 17 kg baboon. [b] Value taken from data collected at ~80 min because the value at 90 min was a negative number.

Table 3. Distribution of [^{11}C]INH Administered iv to Baboons[a]

min after administration	heart	lung	liver	kidney cortex	kidney medulla	plasma
15	0.0103	0.0091	0.0147	0.0177	0.0223	0.00442
	(8.72)	(7.72)	(12.50)	(15.06)	(18.94)	(3.76)
30	0.0072	0.0072	0.0114	0.0109	0.0181	0.00348
	(6.13)	(6.09)	(9.71)	(9.26)	(15.43)	(2.96)
60	0.0044	0.0052	0.0090	0.0091	0.0193	0.00241
	(3.74)	(4.42)	(7.64)	(7.72)	(16.37)	(2.05)
90	0.0049	0.0049	0.0081	0.0100	0.0173	0.0019
	(4.15)	(4.19)	(6.91)	(8.54)	(14.69)	(1.62)

[a] Values given are [%ID/cc] while the values in parentheses are concentration of drug in μg/mL calculated assuming a 5 mg/kg dose and 17 kg baboon.

Table 4. Distribution of [^{11}C]PZA Administered iv to Baboons[a]

min after administration	heart	lung	liver	kidney cortex	kidney medulla	plasma
15	0.0199	0.0103	0.0106	0.0060	0.1815	0.00648
	(67.76)	(35.03)	(36.14)	(20.52)	(617.02)	(22.03)
30	0.0181	0.0078	0.0079	0.0049	0.1395	0.00429
	(61.50)	(26.48)	(26.96)	(16.59)	(474.39)	(14.59)
60	0.0169	0.0065	0.0065	0.0037	0.1009	0.00331
	(57.59)	(22.17)	(21.98)	(12.55)	(343.00)	(11.25)
90	0.0175	0.0055	0.0056	0.0029	0.0675	0.00266
	(59.49)	(18.58)	(19.19)	(9.93)	(229.44)	(9.04)

[a] Values given are [%ID/cc] while the values in parentheses are concentration of drug in μg/mL calculated assuming a 20 mg/kg dose and a 17 kg baboon.

metabolites rapidly penetrates the heart, lung, liver, and kidney. Table 3 gives the estimated concentration of INH in μg/mL at 15, 30, 60, and 90 min following iv administration based on the recommended dose of INH, the weight of the baboon, and assumption that the positron signal derives primarily from the intact drug. The calculated INH concentration is more than 10 times the MIC of this compound against MTB, and hence INH should be a suitable therapy for TB infection as recommended.[8] Barclay and co-workers have shown that the concentration of INH in a surgically removed normal human lung is 1.79 μg/g at about 3 h after iv administration of 108.7 mg INH using [^{14}C]INH as the tracer.[22] In addition, Roth and co-workers have studied the distribution of INH in mice using [^{14}C]INH injected sc and have shown similar drug distributions at 0.5 and 1 h compared to our baboon study assuming that 10 mg/kg drug is administered.[25] Other studies in mice with iv administration show drug concentrations in the liver, lung, and kidney that are several fold higher than the amounts estimated using PET imaging,[34] while Roohi et al. used a technetium-99m derivative of INH to determine the drug biodistribution in Sprague−Dawley rats giving similar drug concentrations in heart and lung but more than 10-fold higher concentrations in the liver and kidney compared to the other studies.[35] Again, interspecies variation could play an important role in any differences observed between our study and those conducted in rodents, with the additional caveat that the study in rats involved the use of INH that had been modified with technetium-99m.

The tissue distribution of [^{11}C]PZA administered iv is shown in Figure 4. The concentration of PZA in μg/mL at 15, 30, 60, and 90 min has been estimated based on the weight of the baboon, the recommended dose of PZA, and the assumption that the positron signal derives primarily from the intact drug (Table 4). The calculated PZA concentration is 1−3 fold higher than the MIC of this compound against MTB. [^{11}C]PZA and/or its radiolabeled metabolites rapidly penetrated the heart, lungs, liver, and kidneys, and in all cases the tissue concentration of PZA exceeded the concentration in serum with the exception of the kidney cortex. The calculated plasma concentration agreed closely with the published value determined in rabbits with iv administration,[36] while the known plasma concentration in humans following oral administration of PZA is about twice that determined in our baboon study.[37] The organ distribution in rabbits has also been examined by dissection and gave a lower concentration of PZA in the lungs, kidneys, and liver compared to that determined in baboons.[36] Because the blood concentration is quite similar in the two studies, the difference in organ distribution could result from differences in drug permeability in the two species. The ability of PZA to cross the blood−brain barrier in rabbits is also quite different because PZA was not observed in the rabbit brain[36] in contrast to our studies and other literature reports.[29] The

concentrations of PZA in baboons determined in the present work are broadly similar to the plasma concentration of PZA determined by MD and HPLC-MS in rats[30] and in humans 1 h after oral administration of 27 mg/kg PZA.[38]

The imaging experiments reported in the present work were conducted using drug administered iv and represent the fate of the drugs once they reach the blood. This is an important point given that the normal route of administration for INH, PZA, and RIF is po. In addition, only micro doses of drugs were used, and we are aware that drug distribution can change as a function of administered dose if one or more processes that affect distribution become saturated. However, on the basis of the mechanism of action of these drugs together with our experience from other drug PK studies, we believe that saturable processes are likely to play only a minor role in modulating distribution. These studies, which were conducted using healthy baboons, thus clearly highlight the utility of using PET imaging to determine drug PK parameters and drug biodistribution noninvasively in vivo and are a prelude to imaging experiments in infected animals and humans. Ultimately, this approach should be useful for determining better TB treatment regimes, especially for disseminated forms of the disease such as CNS TB where assessing drug availability at the site of infection may be difficult. It is also hypothesized that these labeled drugs may be eventually useful for determining the location of bacterial populations in vivo because these drugs are expected to accumulate within the bacteria either by conversion to metabolites that are unable to rapidly leave the cell or by binding with long residence times to their drug targets. Both PZA and INH are prodrugs for which activating enzymes are present in the mycobacterium,[39,40] while the INH-NAD adduct, which is the active form of INH, has a residence time of 60 min on the MTB enoyl-ACP reductase InhA.[41] In addition, RIF is also thought to have a significant residence time on the mycobacterial RNA polymerase based on studies with the *Escherichia coli* homologue which provided a residence time of ~17 min.[42] Importantly, the rapid clearance of all drugs and/or their radiolabeled metabolites from the lungs provides a clear window for imaging populations of TB bacteria because this is the primary site of TB infection.

Conclusions

The front-line TB chemotherapeutics INH, RIF, and PZA have been labeled with carbon-11 and the biodistribution of the labeled drugs has been imaged in baboons in vivo. These PET imaging studies provide an opportunity to review the bioavailability of known drugs both in the brain and peripheral organs, which could potentially improve their use and help to determine the effective dose because these methods can be easily translated to healthy volunteers and patients. Radiosynthesis and formulation of each drug has been accomplished in 1 h, using $[^{11}C]CH_3I$ to label RIF and [^{11}C]HCN to label INH and PZA. Following iv administration, the labeled drugs have been imaged in baboons using PET. INH, PZA, RIF, and/or their radiolabeled metabolites clear rapidly from many tissues, however INH, PZA and/or their radiolabeled metabolites accumulate in the bladder while RIF and/or its radiolabeled metabolites accumulate in the liver and gall bladder, consistent with the routes of excretion of the drugs. In addition, estimates based on the weight of the baboon, a standard drug dose, and the assumption that the positron signal derives primarily from the intact drug indicates that the concentrations of RIF, INH, and PZA in the lungs are at least 10, 10, and 1−3 times higher, respectively, than the MIC values for these drugs against MTB. Furthermore, we find that the ability of the drugs and their radiolabeled metabolites to penetrate the blood−brain barrier decreases in the order PZA > INH > RIF. Estimates of drug concentrations in the brain using the same assumptions outlined above suggest that the concentrations of RIF and INH are 3−4 and >10 times higher than their MIC values, respectively, while PZA is similar to or slightly higher than the MIC. The PK and drug distribution data have important implications for treatment of disseminated TB in the brain and set the scene for imaging the distribution of the pathogen in vivo.

Experimental Section

General. $[^{11}C]CH_3I$ was generated from $[^{11}C]CO_2$ using a PETtrace MeI Microlab (GE Medical System, Milwaukee, WI,). Briefly, $[^{11}C]CO_2$ was obtained from proton bombardment of a N_2/O_2 target ($^{14}N(p,\alpha)^{11}C$) using an EBCO TR 19 cyclotron (Advanced Cyclotron System Inc., Richmond, Canada). $[^{11}C]CO_2$ was heated with H_2 on nickel to produce $[^{11}C]CH_4$, and the latter was converted to $[^{11}C]CH_3I$ by iodination, which was released into a stream of argon.

[^{11}C]HCN was generated from $[^{11}C]CO_2$ using a homemade unit. Briefly, $[^{11}C]CO_2$ was obtained and converted to $[^{11}C]CH_4$ using the same conditions as those used for $[^{11}C]CH_3I$ production. Reaction of $[^{11}C]CH_4$ and NH_3 catalyzed by platinum produced [^{11}C]HCN, which was carried by a stream of argon.

Chemical and radiochemical purity was determined by an analytical HPLC system equipped with both UV and radioactivity detectors. The purities of the intermediate and final products were >95%, and the specific solvent gradients used for each compound are given below.

Synthesis of Demethyl RIF(1) (RIF Precursor). 1-Nitrosopiperazine.[43] Piperazine 0.86 g (10 mmol) in 6N HCl (6 mL) was cooled to −10 °C and a solution of $NaNO_2$ (0.69 g, 10 mmol) in H_2O (12 mL) was added slowly over 1 h. At a temperature below 0 °C, the pH was adjusted to 10 using NaOH, and then the mixture was extracted using chloroform, dried over Na_2SO_4, and the solvent removed by evaporation. The crude product was purified by column chromatography using silica gel and 8% MeOH/CH_2Cl_2 as the mobile phase. The product was a yellow oil, and the yield was 72%. ^{1}H NMR (300 MHz, $CDCl_3$) δ: 4.15−4.18 (m, 2H), 3.74−3.77 (m, 2H), 3.00−3.03 (m, 2H), 2.75−2.79 (m, 2H), 1.83 (s, 1H). ESI-MS calcd for $[M + H]^+$ m/z = 116, found 116.

Demethyl RIF (**1**).[43,44] 1-Nitrosopiperazine 230 mg (2 mmol) was dissolved in 2 mL of THF and was then added slowly to a suspension of $LiAlH_4$ (216 mg, 6 mmol) in 10 mL of THF under N_2 at 0 °C. The mixture was stirred for 5 min and then heated to reflux for 3 h. The cooled reaction mixture was quenched by MeOH until no further gas evolved, concentrated in vacuo, and filtered. The resulting filter cake was washed with MeOH, and the combined filtrate was evaporated to dryness, yielding crude 1-aminopiperazine as a solid. *p*-Toluenesulfonic acid (5 mg), 10 mL of dry THF, and 140 mg of 3-formyl-rifamycin (0.2 mmol) were then added with molecular sieves to the crude 1-aminopiperazine. The reaction mixture was stirred at room temperature overnight, filtered, and concentrated in vacuo. The crude product was purified by column chromatography with silica gel using 5% MeOH/CH_2Cl_2 as the mobile phase. The product was a red solid and the yield was 78%. ^{1}H NMR (600 MHz, $CDCl_3$) δ: 13.15 (s, 1H), 12.01 (s, 1H), 8.30 (s, 1H), 6.57 (dd, J = 15.6, 11.4 Hz, 1H), 6.38 (d, J = 11.4 Hz, 1H), 6.20 (d, J = 12.6 Hz, 1H), 5.93 (dd, J = 15.6 Hz, 4.8 1H), 5.10 (dd, J = 12.6, 6.6 Hz, 1H), 4.94 (d, J = 10.8 Hz, 1H), 3.77 (d, J = 9.0 Hz, 1H), 3.47 (d,

J = 6.6 Hz, 1H), 3.11−3.14 (m, 2H), 3.05−3.06 (m, 2H), 3.04 (s, 3H), 3.01−3.03 (m, 2H), 2.97−3.01 (m, 2H), 2.97−3.06 (m, 1H), 2.33−2.41 (m, 1H), 2.22 (s, 3H), 2.08 (s, 3H), 2.06 (s, 3H), 1.79 (s, 3H), 1.69−1.72 (m, 1H), 1.51−1.56 (m, 1H), 1.33−1.38 (m, 1H), 1.01 (d, J = 7.2 Hz, 3H), 0.88 (d, J = 7.2 Hz, 3H), 0.60 (d, J = 6.6 Hz, 3H), −0.30 (d, J = 6.6 Hz, 3H). ^{13}C NMR (100 MHz, $CDCl_3$) δ 195.12, 174.32, 171.91, 169.50, 169.36, 147.85, 142.60, 142.54, 138.68, 135.02, 134.19, 129.31, 123.18, 120.29, 118.50, 117.87, 112.89, 110.85, 108.74, 106.04, 104.44, 94.39, 77.20, 76.87, 76.77, 74.41, 70.62, 57.09, 53.43, 51.48, 44.82, 39.56, 38.59, 37.55, 33.43, 21.55, 20.80, 17.83, 10.96, 9.02, 8.57, 7.65. ESI-MS calcd for $[M + H]^+$ m/z = 809, found 809. Chemical purity was determined by reverse-phase analytical HPLC using a Phenomenex, Luna C-18, 250 × 4.6, 5 μm column operated at 1 mL/min flow rate using a mobile phase of 32% MeCN/68% H_2O.

Radiosynthesis of [^{11}C]RIF. The synthesis of [^{11}C]RIF was performed using **1** as precursor. A solution of precursor (1.0 mg, 1.2 μmol) was dissolved in 0.1 mL of MeCN and 0.2 mL of DMSO with 0.2 mg of K_2CO_3. After [^{11}C]CH_3I was purged into the solution and trapped, the reaction vessel was sealed and heated at 110 °C for 10 min in an oil bath. The reaction mixture was diluted with 1 mL of aqueous ammonium formate (0.1M) prior to loading onto a semipreparative HPLC column. HPLC purification was performed using a reverse phase C-18 column (Phenomenex, Luna C-18 250 × 10, 5 μm), at a 5 mL/min flow rate with a mobile phase consisting of 35% MeCN/65% aqueous ammonium formate (0.1 M). The product was collected at the expected retention time (17 min), mixed with 100 mg ascorbic acid, and the solvent was removed by rotary evaporation. After dilution with 4 mL of saline, the solution was filtered through an Acrodisc 13 mm syringe filter equipped with a 0.2 μm Supor membrane (Pall Corporation, Ann Arbor, MI) into a sterile vial. Radiochemical purity was determined by reverse-phase analytical HPLC using a Phenomenex, Luna C-18, 250 × 4.6, 5 μm column operated at 1 mL/min flow rate using a mobile phase of 35% MeCN/65% 0.1 M aqueous ammonium formate. Subsequently, purity was verified using TLC (15% MeOH/85% CH_2Cl_2) by cospotting the labeled product with a standard.

Radiosynthesis of [^{11}C]INH. The synthesis of [^{11}C]INH was performed using **2** as the precursor. The precursor (1.0 mg), K_{222} (0.2 mg), and tetrakis(triphenylphosphine)palladium(0) (2.0 mg) was placed in a vial with 0.2 mL of DMSO and heated until all the solid dissolved. This solution was then added to [^{11}C]HCN that had been trapped in 0.1 mL of DMSO, and the reaction mixture was sealed and heated at 135 °C for 5 min. Water (0.3 mL), hydrazine monohydrate (0.3 mL), and NaY zeolite (20 mg) were then added, and after heating for 5 min at 135 °C, acetic acid (0.1 mL) was added. Following an additional 5 min at 135 °C, the reaction mixture was filtered through celite and the reaction vessel was washed with 0.5 mL of water prior to injection onto the semipreparative HPLC column. HPLC purification was performed using a reverse phase PFP column (Phenomenex, Luna PFP(2) 250 × 10, 5 μm) at a 5 mL/min flow rate with a gradient elution: 0−5 min, 100% water; 5−20 min from 100% water to 20% MeCN/80% water. The product was collected at the expected retention time (12 min), and the solvent together with the majority of hydrazine that coeluted was removed by ∼10 min rotary evaporation. After dilution with 4 mL of saline, the solution was filtered through an Acrodisc 13 mm syringe filter equipped with a 0.2 μm Supor membrane into a sterile vial for delivery. Radiochemical purity was determined by reverse-phase analytical HPLC using a Phenomenex, Luna PFP, 250 × 4.6, 5 μm column operated at 1 mL/min with a gradient of 0−20% MeCN in water over 20 min. Subsequently, purity was verified using TLC (25% MeOH/75% CH_2Cl_2) by cospotting the labeled product with a standard.

Quantification of hydrazine in the final formulated solution was determined by modification of a published procedure.[15] Briefly, an aliquot (20 μL) of [^{11}C]INH in saline was added to a test tube containing 20 μL of H_2SO_4 solution (0.1 M) and 20 μL of benzaldehyde in methanol (1 mL benzaldehyde/100 mL methanol). Then 40 μL of sodium borate solution (0.01 M) and 20 μL of methanol was added to the reaction mixture, and 25 μL of this new solution was analyzed using HPLC. The concentration of hydrazine was calculated based on the UV absorption at 313 nm of the hydrazone and by using a standard curve. A blank sample (INH standard without hydrazine) was also analyzed which confirmed that INH did not interfere with the detection of hydrazine.

Radiosynthesis of [^{11}C]PZA. The synthesis of [^{11}C]PZA was performed using **5** as the precursor. The precursor (1.0 mg), K_{222} (0.2 mg), and tetrakis (triphenylphosphine)palladium(0) (2.0 mg) were placed in a vial with 0.2 mL of DMSO and heated until all the solid dissolved. This solution was then added to [^{11}C]HCN that had been trapped in 0.1 mL of DMSO, and the reaction mixture was sealed and heated at 135 °C for 5 min. K_2CO_3 (0.2 mL, 0.1 M) and H_2O_2 (0.1 mL, 30%) were then added, and after heating for 5 min at 135 °C, the reaction mixture was diluted with 0.3 mL of ammonium formate (0.025 M, 5% acetic acid) and filtered through celite. The reaction vessel was washed with 0.5 mL of ammonium formate solution prior to injection onto the semipreparative HPLC column. HPLC purification was performed using a reverse phase PFP column (Phenomenex, Luna PFP(2) 250 × 10, 5 μm) at a 5 mL/min flow rate with a mobile phase consisting of 2% MeCN/98% ammonium formate (0.025M, 5% acetic acid). The product was collected at the expected retention time (7 min), and the solvent was removed by rotary evaporation. After dilution with 4 mL of saline, the solution was filtered through an Acrodisc 13 mm syringe filter equipped with a 0.2 μm Supor membrane into a sterile vial for delivery. Radiochemical purity was determined by reverse-phase analytical HPLC using a Phenomenex, Luna PFP, 250 × 4.6, 5 μm column operated at 1 mL/min with 3% MeCN/97% 0.025 M aqueous ammonium formate as the mobile phase. Subsequently, purity was verified using TLC (25% MeOH/75% CH_2Cl_2) by cospotting the labeled product with a standard.

PET Imaging and Data Processing. Four baboons were included in this study, and all animal experiments were approved by the Brookhaven Institutional Animal Care and Use Committee. Ketamine hydrochloride (10 mg/kg) was administered intramuscularly as an anesthetic agent, and anesthesia was further maintained with oxygen (800 mL/min), nitrous oxide (1500 mL/min), and isoflurane (Forane, 1−4%) during scanning. Two catheters were placed in a radial arm vein and the popliteal artery for [^{11}C]-labeled drug injection and arterial sampling, respectively. Following [^{11}C]-labeled drug injection, arterial blood was collected every 5 s for 2 min, then 2, 5, 10, 20, 30, 45, 60, and 90 min post injection. During the PET scanning, heart rate, respiration rate, body temperature, and pO_2 were monitored. A Siemens HR+ (Siemens high-resolution, whole-body PET scanner with 4.5 mm × 4.5 mm × 4.8 mm resolution at the center of field of view) was used to perform the dynamic PET scans for a total of 90 min with the following time frames in 3D mode: 1 × 10, 12 × 5, 1 × 20, 1 × 30, 8 × 60, 4 × 300, 8 × 450 s. Correction of attenuation was obtained by a transmission scan of a ^{68}Ge rod source prior to each PET scan. Six baboon studies were conducted with average injected doses for RIF, INH, and PZA of 1.54, 4.38, and 5.17 mCi, respectively. Images were reconstructed by filtered back projection (FBP) and analyzed using AMIDE software.[45]

A test tube containing 2.5 mL of octanol and 2.5 mL of phosphate buffer solution (pH 7.4) was mixed with ∼50 μL aliquot of formulated [^{11}C]-labeled drug, vortexed for 2 min and then centrifuged for 2 min to ensure full separation of the aqueous and organic phases. Aliquots from the octanol layer (0.1 mL) and aqueous layer (1 mL) were removed for radioactive counting, while a separate 2 mL aliquot of the octanol layer was carefully transferred to a new test tube containing 0.5 mL of

octanol and 2.5 mL of phosphate buffer (pH 7.4). The octanol phosphate mixture was vortexed and centrifuged, after which a second set of aliquots were obtained. This process was repeated until a total of six sets of samples had been generated. A well counter (Picker, Cleveland, OH) was then used to measure the radioactivity of each sample, and the logD values were calculated using the following equation:

$$\log D = \log(\text{decay-corrected radioactivity in octanol layer} \times 10/\text{decay-corrected radioactivity in phosphate buffer layer})$$

PPB Determination. A 10 μL aliquot of the formulated [^{11}C]-labeled drug was mixed with a sample of baboon plasma (0.8 mL, collected from at least four different baboons and pooled) by gently inverting several times. The mixture was incubated for 10 min at room temperature, and then a 20 μL aliquot was taken to determine the total radioactivity in the plasma sample (A_T; $A_T = A_{bound} + A_{unbound}$). An additional 0.2 mL aliquot of plasma was placed in the upper level of a centrifree tube (Amicon, Inc., Beverly, MA), and then the tube was centrifuged for 10 min. After discarding the upper part of the Centrifree tube, a 20 μL aliquot from the bottom part of the tube was taken to determine the amount of radioactivity that passed through the membrane ($A_{unbound}$). PPB was calculated by the following equation: % unbound = $A_{unbound} \times 100/A_T$.

Metabolite Analysis. Several aliquots (~0.2 mL each) of baboon plasma were collected at various time points during the PET study. Each sample was counted and added to a solution of unlabeled standard (20 μL of a 1 mg/mL solution) in MeCN (0.3 mL). The resulting solution was vortexed and centrifuged, and the supernatant was collected. After mixing with 0.3 mL water, the supernatant was analyzed by HPLC using the following conditions: RIF, Waters μbondapak C-18 3.9 mm × 300 mm column with eluent 70% MeCN/30% 0.1 M aqueous ammonium formate at 1.0 mL/min using UV (254 nm) and radiodetection; INH, Phenomenex spherisorb ODS(2) 4.6 mm × 300 mm, 5 μm column with eluent 2% MeCN/98% 0.02 M aqueous heptane sulfonic acid at 1.0 mL/min using UV (254 nm) and radiodetection; PZA, Phenomenex spherisorb ODS(2) 4.6 mm × 300 mm, 5 μm column with eluent 10% MeCN/90% 0.01 M aqueous potassium phosphate (pH 5.2) at 1.7 mL/min using UV (254 nm) and radiodetection. The percent of unmetabolized radiotracer was determined as the ratio between the fraction of radioactivity coeluting with the unlabeled standard and the total radioactivity from the HPLC column.

Acknowledgment. This work was supported by NIH grant AI084189 to P.J.T. In addition, the work at Brookhaven National Laboratory was performed under contract DE-AC02-98CH10886 with the U.S. Department of Energy, and with infrastructure support from its Office of Biological and Environmental Research. We are grateful to Dr. Michael Schueller for cyclotron operation, David Alexoff for technical assistance with data processing, and the PET radiotracer and imaging team at BNL (Lisa Muench, Pauline Carter, Payton King, and Don Warner) for carrying out primate imaging experiments.

References

(1) Muller, M.; dela Pena, A.; Derendorf, H. Issues in pharmacokinetics and pharmacodynamics of anti-infective agents: distribution in tissue. *Antimicrob. Agents Chemother.* **2004**, *48*, 1441–1453.
(2) Langer, O.; Muller, M. Methods to assess tissue-specific distribution and metabolism of drugs. *Curr. Drug. Metab.* **2004**, *5*, 463–481.
(3) Fischman, A. J.; Alpert, N. M.; Babich, J. W.; Rubin, R. H. The role of positron emission tomography in pharmacokinetic analysis. *Drug Metab. Rev.* **1997**, *29*, 923–956.
(4) Bloom, B. R.; Murray, C. J. Tuberculosis: commentary on a reemergent killer. *Science* **1992**, *257*, 1055–1064.
(5) Kochi, A. The global tuberculosis situation and the new control strategy of the World Health Organization. *Tubercle* **1991**, *72*, 1–6.
(6) Rattan, A.; Kalia, A.; Ahmad, N. Multidrug-resistant *Mycobacterium tuberculosis*: molecular perspectives. *Emerg. Infect. Dis.* **1998**, *4*, 195–209.
(7) Bass, J. B., Jr.; Farer, L. S.; Hopewell, P. C.; O'Brien, R.; Jacobs, R. F.; Ruben, F.; Snider, D. E., Jr.; Thornton, G. Treatment of tuberculosis and tuberculosis infection in adults and children. American Thoracic Society and The Centers for Disease Control and Prevention. *Am. J. Respir. Crit. Care Med.* **1994**, *149*, 1359–1374.
(8) American Thoracic Society. Medical Section of the American Lung Association: Treatment of tuberculosis and tuberculosis infection in adults and children. *Am. Rev. Respir. Dis.* **1986**, *134*, 355−363.
(9) Thwaites, G.; Fisher, M.; Hemingway, C.; Scott, G.; Solomon, T.; Innes, J. British Infection Society guidelines for the diagnosis and treatment of tuberculosis of the central nervous system in adults and children. *J. Infect.* **2009**, *59*, 167–187.
(10) Thwaites, G. E.; Tran, T. H. Tuberculous meningitis: many questions, too few answers. *Lancet Neurol.* **2005**, *4*, 160–170.
(11) Nau, R.; Sorgel, F.; Prange, H. W. Pharmacokinetic optimization of the treatment of bacterial central nervous system infections. *Clin. Pharmacokinet.* **1998**, *35*, 223–246.
(12) Kniess, T.; Rode, K.; Wuest, F. Practical experiences with the synthesis of [^{11}C]CH_3I through gas phase iodination reaction using a TRACERlabFX$_C$ synthesis module. *Appl. Radiat. Isot.* **2008**, *66*, 482–488.
(13) Andersson, I.; Bergstroem, M.; Laanstroem, B. Synthesis of ^{11}C-labelled benzamide compounds as potential tracers for poly(ADP-ribose) synthetase. *Appl. Radiat. Isot.* **1994**, *45*, 707–714.
(14) Milic, D. R.; Opsenica, D. M.; Adnadevic, B.; Solaja, B. A. NaY zeolite: A useful catalyst for nitrile hydrolysis. *Molecules* **2000**, *5*, 118–126.
(15) Elias, G.; Bauer, W. F. Hydrazine determination in sludge samples by high-performance liquid chromatography. *J. Sep. Sci.* **2006**, *29*, 460–464.
(16) Woo, J.; Cheung, W.; Chan, R.; Chan, H. S.; Cheng, A.; Chan, K. In vitro protein binding characteristics of isoniazid, rifampicin, and pyrazinamide to whole plasma, albumin, and α-1-acid glycoprotein. *Clin. Biochem.* **1996**, *29*, 175–177.
(17) Nguyen, D. T.; Guillarme, D.; Rudaz, S.; Veuthey, J. L. Validation of an ultra-fast UPLC-UV method for the separation of antituberculosis tablets. *J. Sep. Sci.* **2008**, *31*, 1050–1056.
(18) Nau, R.; Prange, H. W.; Menck, S.; Kolenda, H.; Visser, K.; Seydel, J. K. Penetration of rifampicin into the cerebrospinal fluid of adults with uninflamed meninges. *J. Antimicrob. Chemother.* **1992**, *29*, 719–724.
(19) McDougall, A. C.; Rose, J. A.; Grahame-Smith, D. G. Penetration of C^{14}-labelled rifampicin into primate peripheral nerve. *Experientia* **1975**, *31*, 1068–1069.
(20) Mindermann, T.; Landolt, H.; Zimmerli, W.; Rajacic, Z.; Gratzl, O. Penetration of rifampicin into the brain tissue and cerebral extracellular space of rats. *J. Antimicrob. Chemother.* **1993**, *31*, 731–737.
(21) Mindermann, T.; Zimmerli, W.; Gratzl, O. Rifampin concentrations in various compartments of the human brain: a novel method for determining drug levels in the cerebral extracellular space. *Antimicrob. Agents Chemother.* **1998**, *42*, 2626–2629.
(22) Barclay, W. R.; Ebert, R. H.; Le Roy, G. V.; Manthei, R. W.; Roth, L. J. Distribution and excretion of radioactive isoniazid in tuberculous patients. *J. Am. Med. Assoc.* **1953**, *151*, 1384–1388.
(23) Barling, R. W.; Selkon, J. B. The penetration of antibiotics into cerebrospinal fluid and brain tissue. *J. Antimicrob. Chemother.* **1978**, *4*, 203–227.
(24) Rouse, D. A.; Li, Z.; Bai, G. H.; Morris, S. L. Characterization of the katG and inhA genes of isoniazid-resistant clinical isolates of *Mycobacterium tuberculosis*. *Antimicrob. Agents Chemother.* **1995**, *39*, 2472–2477.
(25) Roth, L. J.; Manthel, R. W. The distribution of C^{14} labeled isonicotinic acid hydrazide in normal mice. *Proc. Soc. Exp. Biol. Med.* **1952**, *81*, 566–569.
(26) Barlow, C. F.; Schoolar, J. C.; Roth, L. J. Distribution of carbon-14 labeled isoniazid in brain. *Neurology* **1957**, *7*, 820–824.
(27) Schoolar, J. C.; Barlow, C. F.; Roth, L. J. Autoradiography of carbon-14 labeled isoniazid in brain. *Proc. Soc. Exp. Biol. Med.* **1956**, *91*, 347–349.
(28) Ellard, G. A.; Humphries, M. J.; Allen, B. W. Cerebrospinal fluid drug concentrations and the treatment of tuberculous meningitis. *Am. Rev. Respir. Dis.* **1993**, *148*, 650–655.

(29) Forgan-Smith, R.; Ellard, G. A.; Newton, D.; Mitchison, D. A. Pyrazinamide and other drugs in tuberculous meningitis. *Lancet* **1973**, *2*, 374.
(30) Wu, J.-W.; Shih, H.-H.; Wang, S.-C.; Tsai, T.-H. Determination and pharmacokinetic profile of pyrazinamide in rat blood, brain and bile using microdialysis coupled with high-performance liquid chromatography and verified by tandem mass spectrometry. *Anal. Chim. Acta* **2004**, *522*, 231–239.
(31) Nitti, V.; Virgilio, R.; Patricolo, M. R.; Iuliano, A. Pharmacokinetic study of intravenous rifampicin. *Chemotherapy* **1977**, *23*, 1–6.
(32) Furesz, S.; Scotti, R.; Pallanza, R.; Mapelli, E. Rifampicin: a new rifamycin. 3. Absorption, distribution, and elimination in man. *Arzneim. Forsch.* **1967**, *17*, 534–537.
(33) Boman, G. Tissue distribution of ^{14}C-rifampicin II. Accumulation in melanin-containing structures. *Acta Pharmacol. Toxicol.* **1975**, *36*, 267–283.
(34) Verma, R. K.; Kaur, J.; Kumar, K.; Yadav, A. B.; Misra, A. Intracellular time course, pharmacokinetics, and biodistribution of isoniazid and rifabutin following pulmonary delivery of inhalable microparticles to mice. *Antimicrob. Agents Chemother.* **2008**, *52*, 3195–3201.
(35) Roohi, S.; Mushtaq, A.; Jehangir, M.; Malik, S. A. Direct labeling of isoniazid with technetium-99m for diagnosis of tuberculosis. *Radiochim. Acta* **2006**, *94*, 147–152.
(36) Stottmeier, K. D.; Beam, R. E.; Kubica, G. P. The absorption and excretion of pyrazinamide. I. Preliminary study in laboratory animals and in man. *Am. Rev. Respir. Dis.* **1968**, *98*, 70–74.
(37) Peloquin, C. A.; Jaresko, G. S.; Yong, C. L.; Keung, A. C.; Bulpitt, A. E.; Jelliffe, R. W. Population pharmacokinetic modeling of isoniazid, rifampin, and pyrazinamide. *Antimicrob. Agents Chemother.* **1997**, *41*, 2670–2679.
(38) Lacroix, C.; Hoang, T. P.; Nouveau, J.; Guyonnaud, C.; Laine, G.; Duwoos, H.; Lafont, O. Pharmacokinetics of pyrazinamide and its metabolites in healthy subjects. *Eur. J. Clin. Pharmacol.* **1989**, *36*, 395–400.
(39) Zhang, Y.; Heym, B.; Allen, B.; Young, D.; Cole, S. The catalase-peroxidase gene and isoniazid resistance of *Mycobacterium tuberculosis*. *Nature* **1992**, *358*, 591–593.
(40) Blanchard, J. S. Molecular mechanisms of drug resistance in *Mycobacterium tuberculosis*. *Annu. Rev. Biochem.* **1996**, *65*, 215–239.
(41) Rawat, R.; Whitty, A.; Tonge, P. J. The isoniazid-NAD adduct is a slow, tight-binding inhibitor of InhA, the *Mycobacterium tuberculosis* enoyl reductase: adduct affinity and drug resistance. *Proc. Natl. Acad. Sci. U.S.A.* **2003**, *100*, 13881–13886.
(42) Yarbrough, L. R.; Wu, F. Y.; Wu, C. W. Molecular mechanism of the rifampicin−RNA polymerase interaction. *Biochemistry* **1976**, *15*, 2669–2676.
(43) Mao, J.; Wang, Y.; Wan, B.; Kozikowski, A. P.; Franzblau, S. G. Design, synthesis, and pharmacological evaluation of mefloquine-based ligands as novel antituberculosis agents. *ChemMedChem* **2007**, *2*, 1624–1630.
(44) Glamkowski, E. J.; Reitano, P. A.; Woodward, D. L. Synthesis of 3-(4-acylaminopiperazin-1-ylalkyl)indoles as potential antihypertensive agents. *J. Med. Chem.* **1977**, *20*, 1485–1489.
(45) Loening, A. M.; Gambhir, S. S. AMIDE: a free software tool for multimodality medical image analysis. *Mol. Imaging* **2003**, *2*, 131–137.